

## Research Article

**Cite this article:** Scott B, Zaloumis JL, Salifu E, Adegoke AH, Alaufi S, Fraser M, Kavazanjian E and Garcia-Pichel F (2025). Abiotic crust formation in fallow agricultural desert soils through carbonate cementation reduces fugitive dust. *Cambridge Prisms: Drylands*, 2, e3, 1–10 <https://doi.org/10.1017/dry.2024.5>

Received: 09 July 2024

Accepted: 18 October 2024


**Keywords:**

abiotic crust; carbonates; dust storms; fallow land; fugitive dust; management; mechanisms; resistance

**Corresponding author:**

Ferran Garcia-Pichel;  
Email: [ferran@asu.edu](mailto:ferran@asu.edu)

# Abiotic crust formation in fallow agricultural desert soils through carbonate cementation reduces fugitive dust

Brian Scott<sup>1</sup> , Jon L. Zaloumis<sup>2</sup>, Emmanuel Salifu<sup>3</sup>, Adesola H. Adegoke<sup>3</sup>, Salim Alaufi<sup>3</sup>, Matthew Fraser<sup>4</sup>, Edward Kavazanjian<sup>3</sup> and Ferran Garcia-Pichel<sup>5</sup>

<sup>1</sup>Biodesign, Arizona State University, Tempe, AZ, USA; <sup>2</sup>School of Earth and Space Exploration, Arizona State University - Tempe Campus, Tempe, AZ, USA; <sup>3</sup>Center for Bio-mediated and Bio-inspired Geotechnics, Arizona State University, Tempe, AZ, USA; <sup>4</sup>School of Sustainable Engineering and the Built Environment, Arizona State University, Tempe, AZ, USA and <sup>5</sup>Center for Fundamental and Applied Microbiomics, Biodesign Institute, Arizona State University, Tempe, AZ, USA

**Abstract**

Unconsolidated soils typically develop a physical surface crust after wetting and drying. We reproduced this process in the laboratory by wetting with fog and simulated rain on fallow agricultural soils from 26 locations, representing 15 soil types from Pinal County, Arizona. Through correlative analyses, we found that carbonate content was a strong predictor of physical crust strength with fog ( $p < 0.0001$ ,  $R^2 = 0.48$ ) and rain ( $p = 0.004$ ,  $R^2 = 0.30$ ). Clay content increased crust strength ( $p = 0.04$ ) but was not a useful predictor. Our results extend the current understanding of the soil crusting process by highlighting the preeminence of carbonate cementation in desert agricultural soils. Consequently, we identify carbonate as a pragmatic tool for estimating crust strength, a surrogate measure of a soil's potential to produce fugitive dust, which can help prioritize interventions to curb airborne dust in arid lands.

**Impact Statement**

Fugitive dust and dust storms are naturally occurring phenomena in arid and semi-arid environments (Ginoux et al., 2012). Airborne dust has a direct impact on human populations, leading to sometimes fatal traffic accidents (Joshi, 2021; Henry et al., 2023), a variety of respiratory illnesses (Vergadi et al., 2022), and can serve as a vector for plant and animal pathogens (Finn et al., 2021). Human activities like vehicular traffic and plowing can increase dust generation and air particulate loads. Given the size of some dust storms, as large as 160 km in width and 2.4 km in height (Ramakrishnan et al., 2001), efforts to control them may seem futile. While soil stabilization technologies that prevent dust formation are available, their implementation at a large scale is cost-prohibitive (Heredia-Velásquez et al., 2023). Identification of soil stabilization target areas, where intervention would have a high impact, would be very desirable. Our research suggests that carbonate content in dryland agricultural soils is a good predictor of how likely a soil is to become a significant fugitive dust source, and prioritizing the stabilization of soils low in carbonate, or strategically enhancing carbonate precipitation in them, could make interventions more effective.

**Introduction**

Global drylands are commonly characterized by elevated levels of airborne dust that cause a variety of environmental hazards (Middleton, 2017). Dust production can be prevented or diminished by a variety of natural conditions. Vegetation provides a wind break and stabilizes surface soils against wind erosion (Tibke, 1988; Vos et al., 2022). The soil surface itself may be inhabited by biological soil crusts that produce sticky, interwoven cellular material binding particles together (Belnap and Gillette, 1997). Dryland soils may also form a variety of naturally occurring abiotic physical–chemical crusts that provide resistance against wind erosion (Williams et al., 2018).

The mechanisms of abiotic soil crusting have been widely studied. Abiotic crust formation is complex, but in general, crusts develop when fine particles become dispersed in water during rain events, migrate to the soil surface, and infill surficial pores forming a surface seal (Assouline, 2004). Plate-like clays can also align and stack horizontally (Awadhwal and Thierstein, 1985; Williams et al., 2018). Clay dispersion is enhanced by  $\text{Na}^+$  dissolution in low ionic strength rainwater (Forster and Goldberg, 1990). As crust terminology can vary, we use the definitions in (Laker and Nortjé, 2019) and the term “crust formation” to identify that our treatments resulted in a change in crust strength. Crusts formed by clay dispersion are termed depositional. Structural seals, which form under raindrop-induced dispersion, can be amplified when raindrop

© The Author(s), 2024. Published by Cambridge University Press. This is an Open Access article, distributed under the terms of the Creative Commons Attribution-NonCommercial licence (<http://creativecommons.org/licenses/by-nc/4.0/>), which permits non-commercial re-use, distribution, and reproduction in any medium, provided the original article is properly cited. The written permission of Cambridge University Press must be obtained prior to any commercial use.

 Cambridge  
Prisms

 CAMBRIDGE  
UNIVERSITY PRESS

momentum is sufficient to break apart soil aggregates, increasing dispersion (Laker and Nortjé, 2019). While clay minerals (e.g. montmorillonite, kaolinite, and illite) vary in their crust-forming potential due to their differing dispersal behaviors (Forster and Goldberg, 1990), it is difficult to generalize the role of specific mineralogy on crust formation because constituent minerals differ markedly in their response to salts, pH, and organic matter (OM).  $\text{Ca}^{2+}$  (and other polyvalent cations, e.g.  $\text{Mg}^{2+}$ ) generally stabilize the soil by increasing flocculation and aggregate formation (Singer and Warrington, 1992). Calcium (and magnesium) carbonate precipitation may also contribute to crusting through soil cementation (Williams *et al.*, 2018). Carbonates are often a mineral component of soils, particularly in arid and semi-arid environments, and can also act as binding agents increasing crust strength (Gillette *et al.*, 1982). At extremely high carbonate contents, desert soils can form a true pavement (Bungartz *et al.*, 2004). Interventional microbial or enzyme-induced carbonate precipitation (MICP or EICP) for dust control (Hamdan and Kavazanjian, 2016) is also based on carbonate cementation. A correlation between abiotic crusting potential has also been reported with potassium and pH (Stovall *et al.*, 2022).

The presence of an abiotic crust increases the minimal wind velocities required to entrain soil particles in wind flow (Vos *et al.*, 2020) as well as their resistance to abrasion by saltating dust particles (Rice *et al.*, 1996). However, abiotic soil crusts can be disrupted by physical disturbance as is common in agricultural activity (Finn *et al.*, 2021). Due to the large aerial footprint and ongoing disturbance, agricultural fields can be significant dust sources at the landscape scale (Ginoux *et al.*, 2012; Li *et al.*, 2018; Joshi, 2021). Actively cultivated fields have temporarily high dust potential during “fallow” periods between crops (Zucca *et al.*, 2022). A persistent and growing issue in drylands is water scarcity, which extends fallow periods when soil moisture is not replenished through irrigation (Huang *et al.*, 2017). Despite being fallow, dryland fields may continue to be plowed to remove weedy vegetation, for pest control, and in some cases to break up hard soil pans in preparation for future cultivation, a practice known as “preparatory tillage” (Piemeisel *et al.*, 1951; Oswal, 1994). While these practices serve useful purposes, they may render otherwise naturally stable soils into continuous and significant dust sources. Thus, fallow dryland agricultural fields act as increasingly significant sources of atmospheric dust.

We posit that a better mechanistic understanding of crust formation in drylands can be instrumental in predicting the dust-forming potential of soils. Current models, based primarily on fine particle redistribution, are mechanistically accurate but don't predict wind erosion potential. We investigated which, if any, soil compositional factors correlate to soil crust strength. Further, we hypothesized that a soil's carbonate content was most likely to predict abiotic crust formation potential and crust strength. The role of carbonate is independent of mineralogy and raindrop momentum as it relies solely on dissolution (on wetting) and reprecipitation (on drying) at the soil-atmosphere interface (surface cementation). To test our hypothesis, we conducted a study of diverse fallow agricultural soils from Pinal County, Arizona with varying carbonate contents. We generated surface crusts using wetting and drying cycles, with and without raindrop momentum, and measured crust strength. Then we determined which compositional factors were best correlated with the soil's physical crust strength. Our findings shed light on the mechanisms of crust formation contributing to better predicting which soils

are likely dust sources. This, in turn, may help develop land management guidelines that promote superficial abiotic crusting during fallow periods (enough to limit wind erosion) while still meeting the plowman's needs.

## Methods

### Sample locations, sampling, and sample preparation

Composited soil samples (filling a 5-gallon bucket) were collected from 26 fallow agricultural fields with a variety of soil types in Pinal County, Arizona. Sample locations are shown in Figure 1. Soil types (series) were assigned by location based on the United States Department of Agriculture – National Cooperative Soil Survey (NCSS), accessible through the University of California (Davis) online browser (<https://casoilresource.lawr.ucdavis.edu/gmap/>). We selected and sampled 15 soil types to represent a range of relevant physical and chemical properties as listed in Table 1. The sample names are derived from the first three characters of the corresponding soil series name (e.g., Gladsen = Gla), except in the case of Casa Grande (=Cas), which appears at two locations, identified with the numerals “3” and “4” on the NCSS map. Accordingly, these samples are identified as Cas3 and Cas4. In cases where we collected two or more samples within the same soil series name, we added a lower-case identifier [e.g., Cas3(a) and Cas3(f)].

We sampled the upper 5 cm of the soil, sieving samples through a 40 mesh (0.425 mm) screen to remove pre-formed peds, seeds, and very coarse sand, allowing for air drying prior to analysis. Residual soil moisture was determined by drying for 10 min in a microwave oven (Jalilian *et al.*, 2017). In all cases, initial soil moisture was <6.7%. We used the measured residual moisture content to correct gravimetrically determined soil weight.

### Chemical, textural, and structural characterization

The Schiebler volumetric method (ASTM D4373-21) was used to measure soil carbonate in triplicate using an Eijkelkamp Calcimeter. Dry soil specimens were treated with 4 M hydrochloric acid (HCl) to produce  $\text{CO}_2$  gas from carbonates, which was quantified by water displacement. The method was calibrated using commercially obtained calcium carbonate powder. Although the method implies the  $\text{CO}_2$  gas evolves from calcium carbonates, magnesium carbonates may also be detected, thus we specify these results broadly as “carbonate”. Standard geological thin sections (40  $\mu\text{m}$  thick) were prepared from six field-crust soils for microscopic examination using EpoFix epoxy resin (Tippkötter and Ritz, 1996). Epoxy impregnation of the soils was achieved under a vacuum and left to cure overnight. Polished thin sections were prepared commercially by Spectrum Petrographics (Vancouver, WA) and analyzed using a standard dissection and petrographic microscope equipped with cross-polarizers.

Clay content was determined based on grain size using the bouyoucous hydrometer test (ASTM D7928). Other chemical soil tests ( $\text{K}^+$ , pH,  $\text{Na}^+$ ,  $\text{Ca}^{2+}$ ,  $\text{Mg}^{2+}$ , and organic matter) were performed commercially by WARD Laboratories. Three samples were sent to the lab in duplicate to verify sampling and analytical repeatability (Supplemental Table S1). The sodium adsorption ratio (SAR) was calculated as (Brady and Weil, 2008):

$$\text{SAR} = \frac{[\text{Na}^+]}{\sqrt{\frac{1}{2}([\text{Ca}^{2+}] + [\text{Mg}^{2+}])}}$$

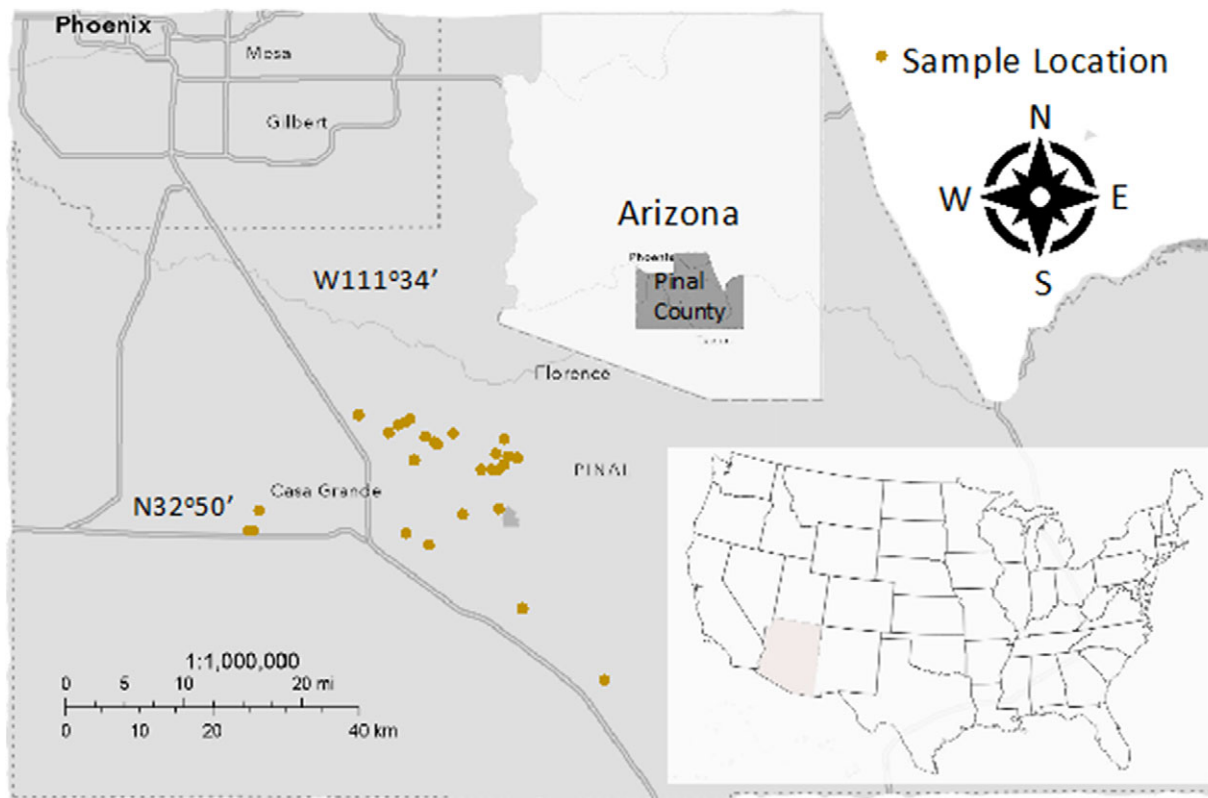


**Figure 1.** Soil sample locations used for this study. All locations are within Pinal County, Arizona. Summer monsoons, the primary source of dust storms, often travel northward through Pinal County into metropolitan Phoenix.

### Penetration resistance (soil surface strength) and soil wetting

The strength of the soil surface was evaluated using an automated Instron penetrometer (Rice et al., 1997; Rice and McEwan, 2001), where a blunt-end probe (6.9 mm diameter) affixed to a loading piston is pushed into the specimen at a constant rate of 1.3 mm/min, while the applied normal force and displacement are recorded continuously. Each specimen was tested multiple times, at least thrice, on visually undisturbed surfaces. The applied force (kiloNewtons) per unit area (square meter) has the units kilo-Pascals (kPa), which were plotted against the displacement (mm). The peak strength of the crust was determined as the average maximum stress (kPa) from the multiple runs.

We evaluated soil crust strength before and after inducing the formation of surface crusts by wetting with deionized water and drying. We used ~150 g of sieved soil (prepared as above) placed in a 100 mm diameter, 20 mm deep Petri dish. Background strength ( $CS_0$ ) was evaluated using dry, sieved soil (not wetted).

Next, the same Petri dish was placed in a 110 cm × 50 cm × 70 cm terrarium provided with a Coospider Reptile Fogger, where a mist was applied until the surface of the soil maintained a visible sheen for more than 10 min, indicating the surficial soil had become nearly saturated. The soil was then dried under an AC Infinity S22 light on a 12-h on–off cycle with a maximum intensity of  $\sim 1000 \mu\text{E m}^{-2} \text{s}^{-1}$ , which created a peak temperature of  $\sim 32^\circ\text{C}$ , for at least two on–off cycles. After drying, the resistance to penetration was measured as above, yielding the fog-induced crust strength ( $CS_F$ ).

Last, we simulated rain-induced crusts by wetting sieved soil to saturation with a PetraTools HD4000 garden sprayer with a fan nozzle. We used the lowest pressure necessary to create a full fan breadth and applied water using a back-and-forth motion from about 10 cm in height, which simulates high-energy raindrops of

$1860 \pm 60 \text{ Joules m}^{-2} \text{ h}^{-1}$  (compared to  $10.3 \pm 0.3 \text{ Joules m}^{-2} \text{ h}^{-1}$  with fog-wetting). Raindrop energy was calculated from the water application rate using equations in (Petrů and Kalibová, 2018). After wetting to saturation, soils were dried, as above, and measured for penetration resistance, yielding the rain-induced crust strength ( $CS_R$ ).

### Threshold velocity (dust generation potential)

A Portable In Situ Soil Wind Erosion Laboratory (PI-SWERL™ – Dust Quant LLC) was used to determine the potential for dust formation by wind shear (Etyemezian et al., 2007). The PI-SWERL™ device (Supplemental Figure S1) is equipped with a rotating flat annular blade in a closed chamber positioned 6 cm above the soil surface. We used six progressive blade rotation speeds: 2000, 3000, 4000, 4500, 5000, and 6000 RPM, for 60 s each. The RPM is converted to frictional velocity, ( $U_*$ ), using equation (1) (Etyemezian et al., 2007).

$$\text{Frictional velocity, } U_* = C_1 \alpha^4 \text{RPM}^{C_2/\alpha} \quad (1)$$

where  $C_1$  is a constant ( $=0.000683$ ),  $C_2$  is a constant ( $=0.832$ ) and the value of  $\alpha$  depends on the surface roughness (taken as 0.992 for the soil types/tests/scenarios in our study).

$U_*$  is then converted to equivalent wind velocities using equation (2) (Marticorena et al., 1997).

$$\text{Wind velocity, } U = \frac{U_*}{k} \ln \frac{z}{z_0} \quad (2)$$

where  $k$  is von Karman's constant (set to 0.4);  $z$  is the height of laminar flow above the ground surface and is taken 1 m (for PI-SWERL™);  $z_0$  is a surface roughness factor and is taken to be 0.001 m for desert landscapes. Laser diffraction is used to

**Table 1.** Soil designations, physical, textural and chemical properties of soil samples in our survey.

| Soil    | Crust strength (kPa) |                 |                 |                  |                  |        | Textural and chemical soil properties |          |     |                       |                        |                        |            |                      |      |
|---------|----------------------|-----------------|-----------------|------------------|------------------|--------|---------------------------------------|----------|-----|-----------------------|------------------------|------------------------|------------|----------------------|------|
|         | Measured values      |                 |                 | Derived values   |                  |        | Measured values                       |          |     |                       |                        |                        | Calculated |                      |      |
|         | CS <sub>0</sub>      | CS <sub>F</sub> | CS <sub>R</sub> | ΔCS <sub>F</sub> | ΔCS <sub>R</sub> | DCS    | Carbonate (%)                         | Clay (%) | pH  | Na <sup>+</sup> (ppm) | Ca <sup>2+</sup> (ppm) | Mg <sup>2+</sup> (ppm) | OM (%)     | K <sup>+</sup> (ppm) | SAR  |
| Cas3(a) | 4.9                  | 134.2           | 373.8           | 129.3            | 368.9            | 239.6  | 0.52                                  | 8.7      | 8.0 | 46                    | 1,768                  | 220                    | 1.7        | 442                  | 1.46 |
| Cas3(b) | 8.1                  | 306.8           | 172.7           | 298.7            | 164.6            | -134.1 | 0.46                                  | 3.8      | 8.3 | 17                    | 1,765                  | 193                    | 0.6        | 310                  | 0.54 |
| Cas3(c) | 18.8                 | 430.3           | 1,069           | 411.5            | 1,050            | 638.8  | 4.62                                  | 16.6     | 8.2 | 265                   | 4,339                  | 454                    | 1.6        | 704                  | 5.41 |
| Cas3(d) | 18.4                 | 319.9           | 479.5           | 301.5            | 461.1            | 159.6  | 1.20                                  | 4.4      | 9.0 | 112                   | 2,894                  | 166                    | 0.6        | 400                  | 2.86 |
| Cas3(e) | 14.7                 | 520.7           | 384.7           | 506.0            | 370.0            | -136.0 | 8.07                                  | 6.3      | 8.5 | 123                   | 3,519                  | 282                    | 1.6        | 970                  | 2.82 |
| Cas3(f) | 17.7                 | 330.5           | 518.8           | 312.8            | 501.1            | 188.3  | 0.47                                  | 6.3      | 8.3 | 37                    | 1,578                  | 180                    | 0.7        | 375                  | 1.25 |
| Cas4(a) | 27.2                 | 494.2           | 652.4           | 467.0            | 625.2            | 158.2  | 5.50                                  | 17.1     | 8.2 | 115                   | 4,890                  | 467                    | 2.5        | 1048                 | 2.22 |
| Con(a)  | 16.9                 | 504.9           | 806.9           | 488.0            | 790.0            | 302.0  | 0.21                                  | 9.4      | 7.7 | 38                    | 1,084                  | 359                    | 1.1        | 633                  | 1.41 |
| Gil(a)  | 4.5                  | 216.8           | 468.5           | 212.3            | 464.0            | 251.7  | 2.32                                  | 11.3     | 8.4 | 195                   | 3,198                  | 366                    | 1.5        | 967                  | 4.62 |
| Gil(b)  | 3.3                  | 411.4           | 828.5           | 408.1            | 825.2            | 417.1  | 3.01                                  | 7.6      | 8.3 | 202                   | 3,661                  | 383                    | 1.8        | 400                  | 4.49 |
| Gin(a)  | 5.9                  | 597.1           | 1,110           | 591.2            | 1,104            | 512.5  | 2.58                                  | 21.9     | 8.5 | 521                   | 5,467                  | 307                    | 2.2        | 572                  | 9.70 |
| Gla(a)  | 5.2                  | 306.7           | 758.3           | 301.5            | 753.1            | 451.6  | 2.27                                  | 25.0     | 8.4 | 165                   | 6,446                  | 283                    | 2.2        | 744                  | 2.84 |
| Gle(a)  | 8.1                  | 374.7           | 533.4           | 366.6            | 525.3            | 158.7  | 2.07                                  | 25.0     | 8.4 | 35                    | 6,676                  | 282                    | 2.1        | 673                  | 0.59 |
| Gle(b)  | 9.9                  | 525.5           | 1,526           | 515.6            | 1,516            | 1,001  | 3.76                                  | 29.8     | 8.1 | 423                   | 5,827                  | 567                    | 2.5        | 1,010                | 7.48 |
| LaP(a)  | 7.4                  | 836.3           | 1,561           | 828.9            | 1,554            | 724.6  | 15.22                                 | 16.4     | 8.8 | 109                   | 3,902                  | 362                    | 1.3        | 468                  | 2.36 |
| LaP(b)  | 1.2                  | 733.8           | 1,562           | 732.6            | 1,561            | 828.0  | 19.47                                 | 9.4      | 8.6 | 221                   | 4,225                  | 428                    | 2.4        | 475                  | 4.58 |
| Lav(a)  | 11.4                 | 556.5           | 1,007           | 545.1            | 995.1            | 450.0  | 10.17                                 | 7.6      | 8.7 | 192                   | 3,850                  | 311                    | 1.6        | 860                  | 4.21 |
| Mar(a)  | 13.2                 | 257.5           | 459.5           | 244.3            | 446.3            | 202.0  | 1.12                                  | 8.8      | 8.1 | 18                    | 3,103                  | 246                    | 0.9        | 353                  | 0.44 |
| Mar(b)  | 15.8                 | 513.3           | 1,065           | 497.5            | 1,049            | 551.5  | 4.92                                  | 9.0      | 8.7 | 192                   | 5,548                  | 288                    | 1.9        | 733                  | 3.55 |
| Mes(a)  | 9.2                  | 291.0           | 1,129           | 281.8            | 1,120            | 837.7  | 1.49                                  | 8.8      | 8.3 | 46                    | 3,099                  | 296                    | 2.0        | 538                  | 1.12 |
| Moh(a)  | 11.0                 | 312.5           | 1,246           | 301.5            | 1,235            | 933.0  | 2.66                                  | 11.9     | 8.6 | 113                   | 3,815                  | 292                    | 1.1        | 712                  | 2.49 |
| Ros(a)  | 8.8                  | 163.3           | 153.0           | 154.5            | 144.2            | -10.3  | 0.17                                  | 3.8      | 8.2 | 6                     | 1,355                  | 97                     | 0.4        | 158                  | 0.22 |
| Tol(a)  | 10.3                 | 266.5           | 1,031           | 256.2            | 1,020            | 764.0  | 5.59                                  | 10.0     | 8.6 | 73                    | 3,767                  | 161                    | 0.8        | 932                  | 1.65 |
| Tol(b)  | 13.6                 | 706.7           | 1,130           | 693.1            | 1,116            | 423.2  | 5.19                                  | 10.0     | 8.3 | 180                   | 3,702                  | 207                    | 1.1        | 1,075                | 4.07 |
| Tol(c)  | 12.5                 | 258.0           | 377.1           | 245.5            | 364.6            | 119.1  | 9.54                                  | 10.2     | 8.1 | 280                   | 4,247                  | 353                    | 1.8        | 497                  | 5.84 |
| Tri(a)  | 7.7                  | 160.0           | 622.0           | 152.3            | 614.3            | 462.0  | 1.95                                  | 17.1     | 8.4 | 250                   | 3,755                  | 326                    | 2.2        | 867                  | 5.53 |

Note: CS<sub>0</sub>, Crust strength of dry, sieved soil measured as penetration resistance in kilopascals (kPa); CS<sub>F</sub>, Crust strength after wetting soil with fog; CS<sub>R</sub>, Crust strength after wetting soil with simulated rain; ΔCS<sub>F</sub>, Increase in crust strength due to fog (CS<sub>F</sub> - CS<sub>0</sub>); ΔCS<sub>R</sub>, Increase in crust strength due to simulated rain (CS<sub>R</sub> - CS<sub>0</sub>); DCS, Differential crust strength due to simulated rain compared to fog (ΔCS<sub>R</sub> - ΔCS<sub>F</sub>); Na<sup>+</sup>, Sodium; Ca<sup>2+</sup>, Calcium; Mg<sup>2+</sup>, Magnesium; SAR, Sodium adsorption ratio; OM, Organic matter; K<sup>+</sup>, Potassium. Shading separates soil types with the same series name.

measure the resulting particle emissions flux (PM10). Each rotor speed corresponds to a specific wind velocity, calculated using internal proprietary software. We report the wind velocity at which soil particles begin to detach, i.e. the threshold velocity (Tv). Laboratory samples for PI-SWERTM testing were prepared by lightly compacting 1.7–1.8 kg of surface soil into a 23 cm diameter × 2.5 cm pie pan and leveling off the surface to minimize surface roughness. The test was initially conducted on dried but untreated specimens and then repeated after creating an abiotic crust by rain-wetting and drying (as detailed for penetrometer testing).

### Data analysis

To determine which chemical and/or physical properties may influence abiotic crusting, we applied linear regression models

using R, open-source statistical analysis software (R-Core, 2017 Version 3.1-3). Linear model homoscedasticity, normality of residuals, and variance inflation factors were evaluated with the “car” package (Fox and Weisberg, 2019). Correlations were performed on the derived values of increased fog-wetted crust strength (ΔCS<sub>F</sub> = CS<sub>F</sub> - CS<sub>0</sub>), increased rain-wetted crust strength (ΔCS<sub>R</sub> = CS<sub>R</sub> - CS<sub>0</sub>), and differential crust strength (DCS: ΔCS<sub>R</sub> - ΔCS<sub>F</sub>) versus each compositional variable. Once the (independent) linear model parameters were determined, we applied the Akaike algorithm (AICcmodavg package version 2.3.3, Mazerolle MJ, 2023) to evaluate which model best described the data (Akaike, 2011). We also considered and reported multi-variate models of regression to determine if they would give a better fit. We considered using transformed data for percent clay content (Lin and Xu, 2020), but this did not have a meaningful impact on overall results.



## Results

### Abiotic crust formation: potential and modes

Abiotic soil crusting was consistently replicated in the laboratory using a wet/dry treatment. Crust formation was evident by comparing the baseline soil strength ( $S_0$ ) of untreated, sieved soil to that attained by fog-wetting and drying ( $CS_F$ ). The magnitude of crusting, determined by penetrometer, varied considerably among samples, between 134 and 836 kPa (Table 1). A second round of crust formation, this time using simulated rainfall to include raindrop momentum in the crusting process ( $CS_R$ ), resulted in penetration forces ranging from 153 to 1562 kPa (Table 1). A single wet/dry cycle sufficed to form a crust, and additional wet/dry cycles did not result in increased strength regardless of watering mode (Supplemental Figure S2). It should also be noted that precipitated calcium carbonate is resilient in an outdoor setting with continued exposure to heat and ultraviolet light radiation (Woolley et al., 2021). In rain-wetted soils of sufficient clay content, a thin surficial clay seal forms that are visible by a characteristic surface sheen when dry, but such clay layers are absent in fog-wetted counterparts. Figure 2 displays these features in prepared petrographic thin sections, where the upper soil profile can be seen in cross-section. These observations are consistent with prior mechanistic notions of crust formation where clays create a depositional soil seal at the surface (Gillette et al., 1982; Laker and Nortjé, 2019). Generally, the net gain in strength of rain-induced crusts ( $\Delta CS_R$ ) was much higher than that of their corresponding fog-induced crust ( $\Delta CS_F$ ), but in 3 out of 26 soils, we found the opposite (Table 1). These soils, Cas3(b), Cas3(e), and Ros(a)] had very low clay content and did not form a clay layer.

We used penetrometer crust strength as a surrogate measure for wind erosion resistance. Prior research (Vos et al., 2020) has shown that penetrometer crust strength can predict the threshold velocity ( $T_v$ ), a direct measure of dust generation potential by wind shear. However, we needed to confirm that this relationship was valid for our soils. Therefore, we conducted both penetrometer and  $T_v$  determinations on a subset of our soil samples. Strength ( $\Delta CS_R$ ) indeed correlated with  $T_v$  (Figure 3;  $R^2 = 0.72$ ,  $p = 0.008$ ), predicting  $T_v$  with a slope of  $4.6 \times 10^{-3} \pm 2.9 \times 10^{-3} \text{ m}^2 \text{ s}^{-1} \text{ kPa}^{-1}$  (95% CI).

### Compositional predictors of soil crust strength

We evaluated the importance of compositional variables that could potentially predict  $CS_F$  and  $CS_R$  by applying a linear correlation model to each variable independently and reporting  $p$  values and slopes with 95% confidence intervals (Table 2). For crust formed by fog watering,  $\Delta CS_F$  was a strong direct function of carbonate content ( $p < 0.0001$ , Table 2, Figure 4a), which spanned a wide range of values from 0.2 to 20% with a median value of 2.6%. Carbonate content was in fact the best predictor among all variables measured. The usefulness of a predictive variable depends not only on the goodness of fit ( $R^2$ ) to a linear model, but also on how far away the slope is from zero. If the slope's 95% CI includes a zero value, the variable has no predictive usefulness. To represent this, we define the Predictive Usefulness Index (PUI) as the ratio of the minimal absolute slope value in the 95% CI range to the best-fit slope. The PUI can range from 1 (best possible predictor) to 0 (useless as a predictor). Carbonate predicts  $\Delta CS_F$  with a PUI of 0.55 (Table 2). While soil pH had a positive correlation with  $\Delta CS_F$  ( $p < 0.05$ ), it provided no predictive usefulness (PUI = 0; Table 2) because its slope 95% CI envelope included a slope of zero. Similarly,  $\text{Mg}^{2+}$  and  $\text{Ca}^{2+}$  were also correlated with  $\Delta CS_F$  though only marginally significant ( $p = 0.10$ ), and PUIs were 0.07 and 0 (Table 2). PUIs are consistent with an Akaike analysis of  $\Delta CS_F$ : the weighted influence of carbonate was 99.79%. We also ran multivariate correlation analyses by combining all variables with carbonate against  $\Delta CS_F$ , and again the model with carbonate alone gave the best fit (Supplemental Table S2). Another consideration is the strength of the linear models, which can be evaluated using homoscedasticity and normality of residuals. Only carbonate met the statistical criteria ( $p < 0.05$ ) for both. We conclude that  $\Delta CS_F$  can only be predicted using carbonate content.

With respect to rain-induced crust strength ( $\Delta CS_R$ ), and considering only single variables, carbonate was also the best predictor of  $\Delta CS_R$  ( $p = 0.004$ , Table 2), the only variable whose linear model met homoscedasticity and normality of residuals criteria, and the one parameter with the highest Akaike weight (42%) and a PUI of 0.36 (Table 2, Figure 4b). Yet, the PUI for  $\Delta CS_R$  carbonate (0.36) was lower than that for  $\Delta CS_F$  carbonate (0.55). Other parameters

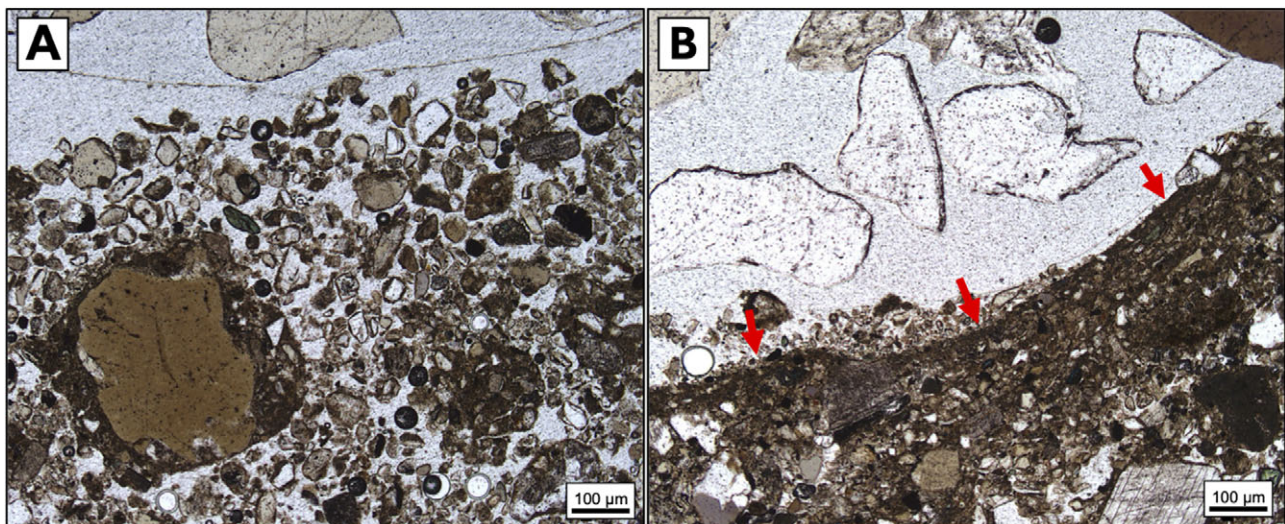


**Figure 2.** Geological thin section photomicrographs showing a cross-sectional profile of Tol(a) soil, a recently fallowed farm plot. (a) Soil collected from an area that had recently been plowed (prior to any subsequent rain events) showing a lack of developed soil crust at the surface (top). (b) Soil collected from the same area after winter rains had created a thin seal layer at the surface (red arrows).

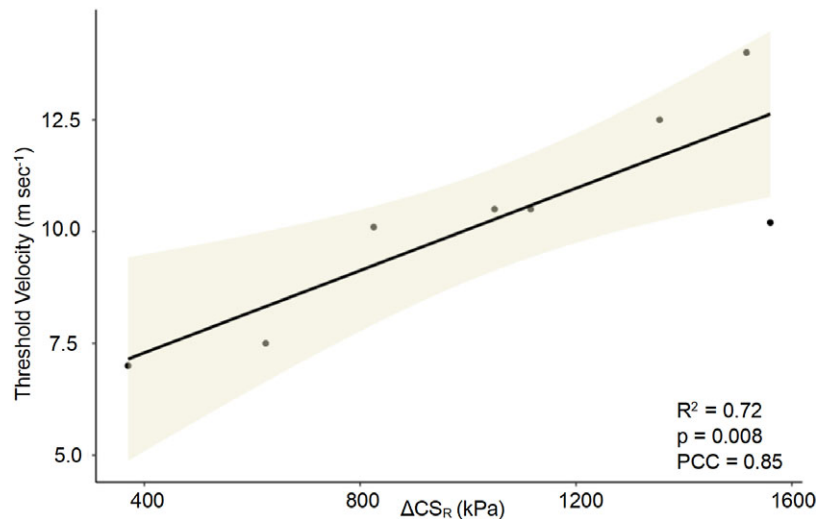


**Figure 3.** Correlation of PI-SWERTL™-determined Threshold Velocity ( $T_v$ ) with penetrometer-measured Rain-Wetted Crust Strength ( $\Delta CS_R$ ). Solid line represents best-fit linear regression, with 95% confidence intervals (shaded area).  $n = 8$ , PCC = Pearson Correlation Coefficient, kPa = kiloPascals.

( $Ca^{2+}$ ,  $Mg^{2+}$ ,  $Na^+$ , clay) had significant ( $p < 0.05$ ) correlations but lower PUIs (Table 2).  $Mg^{2+}$  (PUI = 0.30) and to a lesser degree  $Na^+$  (PUI = 0.20) appeared to be potentially useful as secondary predictors. A multiple regression analysis here shows that Carbonate + Clay (Supplemental Table S2; adjusted  $R^2 = 0.40$ ) provided a better fit than carbonate alone ( $R^2 = 0.30$ ) and had an Akaike-weighted influence of 38%. Thus, while carbonate remains the main driver of  $\Delta CS_R$ , the influence of clays on this parameter seems important as an additional mechanism to increase crust strength (Table 1). However, clay alone is not a useful predictor of  $\Delta CS_R$  (PUI = 0.05, Table 2, Figure 4c). In addition to clay, we considered silt and sand content but did not find a helpful correlation. Sand, silt, and clay values are provided in the Supplemental Table and Figure S3, along with a soil texture triangle.

To further test the notion that clay is important in rain-wetted crust strength, we investigated the relationships of the differential crust strength,  $DCS = \Delta CS_R - \Delta CS_F$ , with potential drivers. These correlations were less robust as all linear models had lower homoscedasticity and normality of residuals ( $p < 0.2$ ). Clay content had the strongest correlation ( $p = 0.04$ , Table 2, Figure 4d), where clay accounted for 27% of the Akaike weighted influence. This is consistent with our structural data in Figure 2. However, clay was not useful as a predictor (PUI = 0.07). The cations  $Ca^{2+}$ ,  $Mg^{2+}$ , and  $Na^+$  seemed to contribute significantly ( $p = 0.04$ ) to the increased strength in rain-induced crusts. Each cation was co-correlated with clay ( $Ca^{2+}$ ,  $p < 0.001$ ;  $Mg^{2+}$ ,  $p = 0.002$ ;  $Na^+$ ,  $p = 0.005$ ), but the variance inflation factors were moderately low (2.54, 1.65, and 1.42, respectively), so independent effects were nevertheless evident. The multiple regression analysis for DCS showed the importance of clay, even when clay + carbonate (adjusted  $R^2 = 0.21$ ) gave a slightly better fit than clay alone ( $R^2 = 0.17$ ; Supplemental Table S2). Thus, while clay appears to be the main driver of DCS, the contribution of carbonate to the clay seal strength seems preeminent in terms of predictive value.

## Discussion

We show that carbonate content can be used as a predictor of abiotic crust formation and strength in dryland farm soils from Pinal County in Arizona, and by deduction, to predict their potential as a source of wind-blown dust. Our experiments show that,

following a soil-wetting event, drying causes carbonate (re)precipitation and soil cementation. This likely happens more prominently at the soil surface where water evaporation raises effective concentrations of carbonate and cations beyond their respective salt's solubility products, promoting preferentially surface cementation, as a drop in water potential promotes upward flux of the soil solution to continuously feed the process. The current mechanistic framework for soil crust formation, based primarily on studies that focus on water infiltration, tends to emphasize clay re-deposition and sealing (Assouline, 2004; Cattle *et al.*, 2004) and downplays the role of cementation. Cementation has not been shown to be a factor in infiltration rates but effectively stabilizes soil against wind erosion (McFadden *et al.*, 1998; Robinson and Woodun, 2008). We saw a very high degree of correlation (Table 2;  $p < 0.0001$ ) between fog-wetted strength ( $CS_F$ ) and carbonate, and virtually exclusive dependence on this parameter. This conclusion is also supported indirectly by the positive relationship of pH to crust strength.  $CS_F$  had a highly significant ( $p < 0.05$ , Table 2) correlation with pH, as alkalization increases the proportion of carbonate ions in solution, promoting precipitation, even within an invariant level of dissolved inorganic carbon (Stumm and Morgan, 1996). This effect did not overwhelm the importance of the absolute carbonate content, and pH did not rise to the level of a good predictor. Similarly, divalent cation levels can be expected to correlate with crust strength, as they also influence how easily soil solution concentrations exceed the solubility product for carbonate minerals. Indeed,  $\Delta CS_R$  had a high correlation with  $Mg^{2+}$ , and  $Ca^{2+}$  ( $p < 0.03$ , Table 2). We acknowledge that others have speculated on the role of carbonates in soil crusting (Gillette *et al.*, 1982; Robinson and Woodun, 2008; Virto *et al.*, 2011; Feng *et al.*, 2013), though without thorough experimental interrogations. By contrast, the correlation between crust strength and clay content was weak. Hence, abiotic crust strength is primarily controlled by carbonate precipitation, while clay sealing has a secondary effect that increases strength. By isolating the factors that cause deposition and cementation processes, our results not only point to a useful predictive tool but suggest carbonate precipitation may be an important factor to consider when evaluating the potential abiotic crust strength of desert farm soils, and possibly other settings with frequent disturbance such as off-road areas and military training grounds.

**Table 2.** Correlation of soil crust strength parameters with single primary predictive variables

|                        | PCC         | p                 | R <sup>2</sup> | Slope              | PUI         | Akaike %<br>(single variable) |
|------------------------|-------------|-------------------|----------------|--------------------|-------------|-------------------------------|
| Fog ( $\Delta CS_F$ )  |             |                   |                |                    |             |                               |
| <b>Carbonate</b>       | <b>0.69</b> | <b>&lt;0.0001</b> | <b>0.48</b>    | <b>26.6 ± 11.9</b> | <b>0.55</b> | 0.9979                        |
| pH                     | 0.37        | <0.05             | 0.14           | 192 ± 268          | 0           | 0.9985                        |
| Ca <sup>2+</sup>       | 0.31        | 0.10              | 0.10           | 0.040 ± 0.049      | 0           | 0.9988                        |
| Mg <sup>2+</sup>       | 0.31        | 0.10              | 0.10           | 0.71 ± 0.66        | 0.07        | 0.9992                        |
| Na <sup>+</sup>        | 0.29        | 0.13              | 0.08           | 0.51 ± 0.58        | 0           | 0.9994                        |
| SAR                    | 0.28        | 0.15              | 0.08           | 26.4 ± 31.4        | 0           | 0.9997                        |
| OM                     | 0.21        | 0.28              | 0.04           | 78 ± 117           | 0           | 0.9998                        |
| Clay                   | 0.13        | 0.52              | 0.02           | 5.5 ± 10.9         | 0           | 0.9999                        |
| K <sup>+</sup>         | 0.13        | 0.50              | 0.02           | 0.17 ± 0.29        | 0           | 1.0000                        |
| Rain ( $\Delta CS_R$ ) |             |                   |                |                    |             |                               |
| <b>Carbonate</b>       | <b>0.55</b> | <b>0.004</b>      | <b>0.30</b>    | <b>48.1 ± 31.0</b> | <b>0.36</b> | 0.42                          |
| Mg <sup>2+</sup>       | 0.46        | 0.006             | 0.27           | 2.0 ± 1.4          | 0.30        | 0.69                          |
| Na <sup>+</sup>        | 0.29        | 0.02              | 0.21           | 1.5 ± 1.2          | 0.20        | 0.78                          |
| Ca <sup>2+</sup>       | 0.43        | 0.03              | 0.19           | 0.12 ± 0.11        | 0.08        | 0.84                          |
| SAR                    | 0.43        | 0.03              | 0.18           | 76.9 ± 68.2        | 0.11        | 0.89                          |
| Clay                   | 0.41        | 0.04              | 0.16           | 24.2 ± 23.1        | 0.05        | 0.93                          |
| OM                     | 0.40        | 0.05              | 0.16           | 259 ± 254          | 0.02        | 0.97                          |
| K <sup>+</sup>         | 0.31        | 0.13              | 0.09           | 0.50 ± 0.65        | 0           | 0.99                          |
| pH                     | 0.29        | 0.15              | 0.09           | 442 ± 606          | 0           | 1.00                          |
| Rain – Fog (DCS)       |             |                   |                |                    |             |                               |
| <b>Clay</b>            | <b>0.41</b> | <b>0.04</b>       | <b>0.17</b>    | <b>18.8 ± 17.4</b> | <b>0.07</b> | 0.27                          |
| Ca <sup>2+</sup>       | 0.39        | 0.04              | 0.15           | 0.08 ± 0.08        | 0           | 0.42                          |
| Na <sup>+</sup>        | 0.39        | 0.04              | 0.15           | 1.0 ± 0.58         | 0.42        | 0.56                          |
| Mg <sup>2+</sup>       | 0.39        | 0.04              | 0.15           | 1.33 ± 1.11        | 0.17        | 0.70                          |
| SAR                    | 0.35        | 0.06              | 0.12           | 50.5 ± 53.2        | 0           | 0.79                          |
| Carbonate              | 0.32        | 0.09              | 0.11           | 21.5 ± 26.6        | 0           | 0.86                          |
| OM                     | 0.32        | 0.09              | 0.10           | 181 ± 195          | 0           | 0.92                          |
| K <sup>+</sup>         | 0.30        | 0.12              | 0.09           | 0.32 ± 0.50        | 0           | 0.97                          |
| pH                     | 0.29        | 0.23              | 0.05           | 250 ± 470          | 0           | 1.00                          |

Note: Soil crust strength measures are:  $\Delta CS_F$ , Fog-wetted strength;  $\Delta CS_R$ , Rain-wetted strength; DCS, Differential crust strength (Rain – Fog). Among variables: SAR, Sodium adsorption ratio; OM, Organic matter. Listed statistics are the Pearson Correlation Coefficient (PCC) for a linear model, the probability that there is no correlation ( $p$ ), the goodness of linear fit ( $R^2$ ), and the best-fit slope (slope), representing the change in strength divided by the change in the explanatory variable value, with its 95% confidence interval. Slope units vary: Carbonate + Clay = kPa/(g/100 g soil); cations and OM = kPa/(g/1 × 10<sup>6</sup> g soil); pH + SAR = kPa/(unitless). PUI stands for Predictive Usefulness Index, which is calculated as the ratio of the minimal absolute slope value in the 95% CI range to the best-fit slope and varies from 1 (best possible predictor) to 0 (useless as a predictor). Akaike weights depict the cumulative contribution of each additional variable to the percent of variation predicted by the primary variable (bolded) in order of decreasing contributions.

By comparing fog-wetted to rain-wetted soils, we were able to parse out cementation due to carbonate precipitation, eliminating raindrop energy as a factor needed to break apart and disperse aggregate-bound clays (McIntyre, 1958). Comparisons of fog and rain-wetting used in the past have been applied to study infiltration rates, not crusting (Kaseke et al., 2012; Li et al., 2018), where rain-wetting decreases infiltration (Agassi et al., 1985). In these cases, the authors report how dispersed clays and sodium combine to create a water-resistant soil seal (Khatei et al., 2024), but cementation was not considered. Consistent with this canonical mechanistic framework based on the formation of a depositional clay seal, DCS was

most strongly correlated with clay ( $p = 0.04$ , Table 2). If clay sealing were the principal mechanism of increased crust strength, one should expect the content of Na<sup>+</sup> to be also important, because it acts as a clay dispersing agent (Parameswaran and Sivapullaiah, 2017). Indeed, in our study, Na<sup>+</sup> was also correlated with strength and is potentially a useful predictor of DCS (PUI = 0.42, Table 2).

Our study presents a unique condition by using exclusively arid agricultural soils and considering crust strength by wetting with and without forceful rain impact. Prior mechanistic studies have largely considered how the destructive force of raindrops destroys soil aggregates (McIntyre, 1958; Fan et al., 2008; Feng et al., 2013).



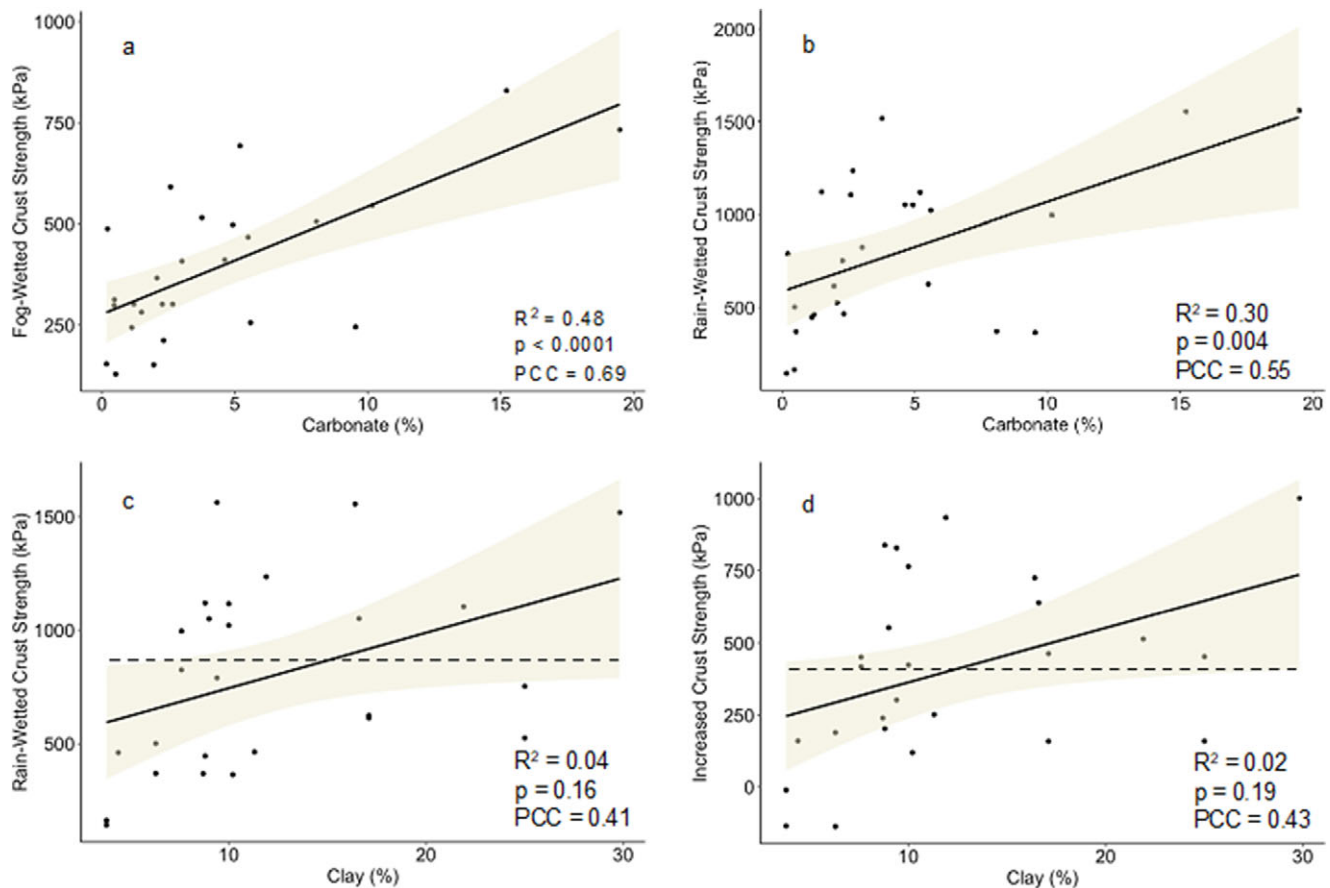


**Figure 4.** Best-fit models for abiotic crust strength as a function of predictive variables. PCC = Pearson Correlation Coefficient, kPa = kiloPascals. The solid line represents the best-fit linear model. The shaded area shows the 95% Confidence Interval for the slope ( $n = 26$ ). The dashed line in (c) shows that the range includes a slope of 0 (Predictive Usefulness Index (PUI) = 0) and therefore is useless as a predictor. The comparable dashed line in (d) has a very small positive slope (PUI = 0.07) and therefore has minimal usefulness as a predictor.

In our setting, the soils had a low degree of aggregation after dry season plowing. We removed even small aggregates in our experiment by sieving. Thus, the experimental conditions may have dampened a larger effect of raindrop energy potentially present in non-agricultural soils. In addition, the aridisols we targeted may have enhanced the role of carbonate precipitation and cementation due to their alkaline nature and high content of calcium, magnesium, and carbonate ions (Dunkerley, 2011). In such soils, processes that stabilize soil by increasing flocculation and aggregate formation (Singer and Warrington, 1992) may not be as relevant.

While our study has implications for the mechanisms of desert soil crust formation, our primary objective was to find a predictive tool to estimate abiotic crust strength as a tool to aid in dust control measures. To that end, we have shown that in desert agricultural soils carbonate is the best predictor of crust strength, a surrogate for dust-forming potential (Rice *et al.*, 1997) (Figure 3). While we obtained a favorable correlation of crust strength and Tv for dust formation ( $p = 0.008$ , Figure 3), we acknowledge the limitations of our findings. PI-SWERL™ results require expertise to interpret (Supplemental Figure S4), and penetrometer tests can be variable, with the potential for false positives and outliers (Supplemental Figure S5). In addition, we extended our dust susceptibility prediction across two correlative steps (carbonate to  $CS_R$  and to dust formation potential).

We contend that fugitive dust control in large areas such as Pinal County can be optimized by identification of soils with low crusting potential, and prioritizing interventions there. In this regard, the soil's carbonate content constitutes a suitable screening parameter that is

measurable with simple, portable tests. Some carbonate content data is immediately available in public databases, such as the USGS Soil Survey, although local carbonate testing would be prudent since soils within a single type can be variable in carbonate content and dust susceptibility (for example, consider the Cas3 series in Table 1). It is possible to map the estimated wind erodibility of soils based on carbonate content. We provide an example in Supplemental Figure S6. Previous work on modeling aeolian dust concentrations in Pinal County, using soil texture, met with limited success (Joshi, 2021). Our work suggests that the inclusion of carbonate content may improve such efforts. We note here that such a model would only predict dust potential from undisturbed soils because continual disturbance by plowing effectively destroys the soil armor. Based on our lab and field observations, all disturbed soils are potential dust sources, thus both soil stabilization and modified farming practices in fallow fields are required for effective dust mitigation strategies.

**Open peer review.** For open peer review materials, please visit <https://doi.org/10.1017/dry.2024.5>.

**Supplementary material.** To view supplementary material for this article, please visit <http://doi.org/10.1017/dry.2024.5>.

**Data Availability statement.** All results are listed in Table 1 and Supplementary Table S1.

**Acknowledgments.** Paco Ollerton helped us navigate within the Pinal County farming community, and, as a member of the ADEQ Agricultural PM10 Best



Management Practices Committee for dust control, provided insight into existing dust control efforts. Dr. Xi Yu performed some of the lab testing and analysis and Dr. Pierre Herckes provided helpful editorial comments. We thank Dr. Tom Sharp and Leah Shetyanman for access and assistance in the petrographic microscopy laboratory at Arizona State University.

**Author Contribution.** BS and FGP prepared the manuscript, with sections contributed by ES. FGP directed the research. EK and ES directed the penetrometer and PI-SWERM™ testing and, along with MF, provided manuscript edits. SAA and AHA performed the penetrometer and PI-SWERM™ testing. JLZ coordinated soil thin section mounts and accompanying microscopy.

**Financial Support.** Funding for this research was provided by a grant from the Arizona Board of Regents (#31).

**Competing interest.** None.

## References

- Agassi M, Morin J and Shainberg I (1985) Effect of raindrop impact energy and water salinity on infiltration rates of sodic soils. *SSSAJ* 49, 186–190.
- Akaike H (2011) Akaike's information criterion. *International Encyclopedia of Statistical Science*, 25.
- Assouline S (2004) Rainfall-induced soil surface sealing: A critical review of observations, conceptual models, and solutions. *Vadose Zone Journal* 3, 570–591.
- Awadhwal NK and Thierstein GE (1985) Soil crust and its impact on crop establishment: A review. *Soil and Tillage Research* 5(3), 289–302. [https://doi.org/10.1016/0167-1987\(85\)90021-2](https://doi.org/10.1016/0167-1987(85)90021-2).
- Belnap J and Gillette DA (1997) Disturbance of biological soil crusts: Impacts on potential wind erodibility of sandy desert soils in southeastern Utah. *Land Degradation & Development* 8(4), 355–362. [https://doi.org/10.1002/\(SICI\)1099-145X\(199712\)8:4<355::AID-LDR266>3.0.CO;2-H](https://doi.org/10.1002/(SICI)1099-145X(199712)8:4<355::AID-LDR266>3.0.CO;2-H).
- Brady NC and Weil RR (2008) *The Nature and Properties of Soils*, Rev. 14th edn. Upper Saddle River, NJ: Pearson Prentice Hall.
- Burgart F, Garvie LAJ and Nash TH (2004) Anatomy of the endolithic Sonoran Desert lichen *Verrucaria rubrocincta* Breuss: implications for biodegradation and biomineralization. *The Lichenologist* 36(1), 55–73. <https://doi.org/10.1017/s0024282904013854>.
- Cattle S, Cousin I, Darboux F and Bissonnais YL (2004) The effect of soil crust ageing, through wetting and drying, on some surface structural properties.
- Dunkerley DL (2011) Desert Soils. In Thomas DSG (ed), *Arid Zone Geomorphology*. 1 ed.: Wiley, 101–129.
- Etyemezian V, Nikolich G, Ahonen S, Pitchford M, Sweeney M, Purcell R, Gillies J and Kuhns H (2007) The portable in situ wind Erosion Laboratory (PI-SWERM): A new method to measure PM10 windblown dust properties and potential for emissions. *Atmospheric Environment* 41(18), 3789–3796. <https://doi.org/10.1016/j.atmosenv.2007.01.018>.
- Fan Y, Lei T, Shainberg I and Cai Q (2008) Wetting rate and rain depth effects on crust strength and micromorphology. *Soil Science Society of America Journal* 72(6), 1604–1610. <https://doi.org/10.2136/sssaj2007.0334>.
- Feng G, Sharratt B and Vaddella V (2013) Windblown soil crust formation under light rainfall in a semiarid region. *Soil and Tillage Research* 128, 91–96. <https://doi.org/10.1016/j.still.2012.11.004>.
- Finn DR, Maldonado J, de Martini F, Yu J, Penton CR, Fontenele RS, Schmidlin K, Kraberger S, Varsani A, Gile GH, Barker B, Kollath DR, Muenich RL, Herckes P, Fraser M and Garcia-Pichel F (2021) Agricultural practices drive biological loads, seasonal patterns and potential pathogens in the aerobiome of a mixed-land-use dryland. *Science of the Total Environment* 798, 149239. <https://doi.org/10.1016/j.scitotenv.2021.149239>.
- Forster S and Goldberg HS (1990) Flocculation of reference clays and arid-zone soil clays. *Soil Science Society of America Journal* 54, 714–718.
- Fox J and Weisberg S (2019) *An R Companion to Applied Regression*, 3rd edn. Thousand Oaks, CA: Sage.
- Gillette DA, Adams J, Muhs D and Kihl R (1982) Threshold friction velocities and rupture moduli for crusted desert soils for the input of soil particles into the air. *Journal of Geophysical Research* 87(C11), 9003. <https://doi.org/10.1029/JC087iC11p09003>.
- Ginoux P, Prospero JM, Gill TE, Hsu NC and Zhao M (2012) Global-scale attribution of anthropogenic and natural dust sources and their emission rates based on MODIS Deep Blue aerosol products: Anthropogenic and natural dust sources. *Reviews of Geophysics* 50(3). <https://doi.org/10.1029/2012RG000388>.
- Hamdan N and Kavazanjian E (2016) Enzyme-induced carbonate mineral precipitation for fugitive dust control. *Géotechnique* 66(7), 546–555. <https://doi.org/10.1680/jgeot.15.P.168>.
- Henry MB, Mozer M, Rogich JJ, Farrell K, Sachs JW, Selzer J, Chikani V, Bradley G and Comp G (2023) Haboob dust storms and motor vehicle collision-related Trauma in Phoenix, Arizona. *Western Journal of Emergency Medicine* 24(4). <https://doi.org/10.5811/WESTJEM.59381>.
- Heredia-Velásquez AM, Giraldo-Silva A, Nelson C, Bethany J, Kut P, González-de-Salceda L and Garcia-Pichel F (2023) Dual use of solar power plants as biocrust nurseries for large-scale arid soil restoration. *Nature Sustainability* 6(8), 955–964. <https://doi.org/10.1038/s41893-023-01106-8>.
- Huang J, Li Y, Fu C, Chen F, Fu Q, Dai A, Shinoda M, Ma Z, Guo W, Li Z, Zhang L, Liu Y, Yu H, He Y, Xie Y, Guan X, Ji M, Lin L, Wang S, Yan H and Wang G (2017) Dryland climate change: Recent progress and challenges. *Reviews of Geophysics* 55(3), 719–778. <https://doi.org/10.1002/2016rg000550>.
- Jalilian J, Moghaddam SS and Tagizadeh Y (2017) Accelerating soil moisture determination with microwave oven. *Journal of Chinese Soil and Water Conservation* 48(2), 101–103.
- Joshi JR (2021) Quantifying the impact of cropland wind erosion on air quality: A high-resolution modeling case study of an Arizona dust storm. *Atmospheric Environment* 263, 118658. <https://doi.org/10.1016/j.atmosenv.2021.118658>.
- Kaseke KF, Mills AJ, Esler K, Henschel J, Seely MK and Brown R (2012) Spatial variation of “Non-Rainfall” water input and the effect of mechanical soil crusts on input and evaporation. *Pure and Applied Geophysics* 169(12), 2217–2229. <https://doi.org/10.1007/s00024-012-0469-5>.
- Khatei G, Rinaldo T, Van Pelt RS, D’Odorico P and Ravi S (2024) Wind erodibility and particulate matter emissions of salt-affected soils: The case of dry soils in a low humidity atmosphere. *Journal of Geophysical Research: Atmospheres* 129(1). <https://doi.org/10.1029/2023jd039576>.
- Laker MC and Nortjé GP (2019) Review of existing knowledge on soil crusting in South Africa. In *Advances in Agronomy*. Elsevier, pp. 189–242.
- Li J, Kandakji T, Lee JA, Tatarko J, Blackwell J, Gill TE and Collins JD (2018) Blowing dust and highway safety in the southwestern United States: Characteristics of dust emission “hotspots” and management implications. *Science of the Total Environment* 621, 1023–1032. <https://doi.org/10.1016/j.scitotenv.2017.10.124>.
- Lin L and Xu C (2020) Arcsine-based transformations for meta-analysis of proportions: Pros, cons, and alternatives. *Health Science Reports* 3(3), e178. <https://doi.org/10.1002/hsr2.178>.
- Marticoarena B, Bergametti G, Aumont B, Callot Y, N’Doumé C and Legrand M (1997) Modeling the atmospheric dust cycle: 2. Simulation of Saharan dust sources. *Journal of Geophysical Research: Atmospheres* 102(D4), 4387–4404. <https://doi.org/10.1029/96jd02964>.
- McFadden LD, McDonald EV, Wells SG, Anderson K, Quade J and Forman SL (1998) The vesicular layer and carbonate collars of desert soils and pavements: formation, age and relation to climate change. *Geomorphology* 24(2–3), 101–145. [https://doi.org/10.1016/S0169-555X\(97\)00095-0](https://doi.org/10.1016/S0169-555X(97)00095-0).
- McIntyre DS (1958) Permeability measurements of soil crusts formed by raindrop impact. *Soil science* 85(4), 185–189.
- Middleton NJ (2017) Desert dust hazards: A global review. *Aeolian Research* 24, 53–63. <https://doi.org/10.1016/j.aeolia.2016.12.001>.
- Oswal MC (1994) Water conservation and dryland crop production in arid and semi-arid regions. *Annals of Arid Zone* 33(2), 95–104.
- Parameswaran TG and Sivapullaiah PV (2017) Influence of sodium and lithium monovalent cations on dispersivity of clay soil. *Journal of Materials in Civil Engineering* 29(7). [https://doi.org/10.1061/\(ASCE\)MT.1943-5533.000187](https://doi.org/10.1061/(ASCE)MT.1943-5533.000187).
- Petrů J and Kalibová J (2018) Measurement and computation of kinetic energy of simulated rainfall in comparison with natural rainfall. *Soil and Water Research* 13(4), 226–233. <https://doi.org/10.17221/218/2016-swr>.
- Piemeisel RL, Lawson FR and Carsner E (1951) Weeds, insects, plant diseases, and dust storms. *Science* 73(2).

- R-Core T** (2017) A language and environment for statistical computing. In: *R Foundation for Statistical Computing*, Vienna, Austria.
- Ramakrishnan B, Lueders T, Dun PF and Friedrich MW** (2001) Archaeal community structures in rice soils from different geographical regions before and after initiation of methane production. *FEMS Microbiology Ecology* **37**, 12.
- Rice MA and McEwan IK** (2001) Crust strength: a wind tunnel study of the effect of impact by saltating particles on cohesive soil surfaces. *Earth Surface Processes and Landforms* **26**(7), 721–733. <https://doi.org/10.1002/esp.217>.
- Rice MA, Mullins CE and McEwan IK** (1997) An analysis of soil crust strength in relation to potential abrasion by saltating particles. *Earth Surface Processes and Landforms* **22**(9), 869–883. [https://doi.org/10.1002/\(SICI\)1096-9837\(199709\)22:9<869::AID-ESP785>3.0.CO;2-P](https://doi.org/10.1002/(SICI)1096-9837(199709)22:9<869::AID-ESP785>3.0.CO;2-P).
- Rice MA, Willetts BB and McEwan IK** (1996) Wind erosion of crusted sediment soils. *Earth Surface Processes and Landforms* **21**(3), 279–293. [https://doi.org/10.1002/\(SICI\)1096-9837\(199603\)21:3<279::AID-ESP633>3.0.CO;2-A](https://doi.org/10.1002/(SICI)1096-9837(199603)21:3<279::AID-ESP633>3.0.CO;2-A).
- Robinson DA and Woodun JK** (2008) An experimental study of crust development on chalk downland soils and their impact on runoff and erosion. *European Journal of Soil Science* **59**(4), 784–798. <https://doi.org/10.1111/j.1365-2389.2008.01033.x>.
- Singer MJ and Warrington DN** (1992) Crusting in the Western United States. In Summer ME and Stewart BA (eds), *Soil Crusting: Chemical and Physical Processes*. Lewis Publishers, Boca Raton, FL.
- Stovall MS, Ganguli AC, Schallner JW, Faist AM, Yu Q and Pietrasiak N** (2022) Can biological soil crusts be prominent landscape components in rangelands? A case study from New Mexico, USA. *Geoderma* **410**, 115658. <https://doi.org/10.1016/j.geoderma.2021.115658>.
- Stumm W and Morgan JJ** (1996) *Aquatic Chemistry. Chemical Equilibria and Rates in Natural Waters*, 3rd edn. John Wiley & Sons, Inc.
- Tibke G** (1988) Basic principles of wind erosion control. *Agriculture, Ecosystems and Environment* **22/23**, 103–122.
- Tippkötter R and Ritz K** (1996) Evaluation of polyester, epoxy and acrylic resins for suitability in preparation of soil thin sections for in situ biological studies. *Geoderma* **69**(1), 31–57. [https://doi.org/10.1016/0016-7061\(95\)00041-0](https://doi.org/10.1016/0016-7061(95)00041-0).
- Vergadi E, Rouva G, Angeli M and Galanakis E** (2022) Infectious diseases associated with desert dust outbreaks: A systematic review. *International Journal of Environmental Research and Public Health* **19**(11), 6907. <https://doi.org/10.3390/ijerph19116907>.
- Virto I, Gartzia-Bengoetxea N and Fernández-Ugalde O** (2011) Role of organic matter and carbonates in soil aggregation estimated using laser diffractometry. *Pedosphere* **21**(5), 566–572. [https://doi.org/10.1016/S1002-0160\(11\)60158-6](https://doi.org/10.1016/S1002-0160(11)60158-6).
- Vos H, Fister W, Eckardt F, Palmer A and Kuhn N** (2020) Physical crust formation on sandy soils and their potential to reduce dust emissions from croplands. *Land* **9**(12), 503. <https://doi.org/10.3390/land9120503>.
- Vos HC, Karst IG, Eckardt FD, Fister W and Kuhn NJ** (2022) Influence of crop and land management on wind erosion from sandy soils in dryland agriculture. *Agronomy* **12**(2), 457. <https://doi.org/10.3390/agronomy12020457>.
- Williams AJ, Pagliai M and Stoops G** (2018) Physical and biological surface crusts and seals. In *Interpretation of Micromorphological Features of Soils and Regoliths*, Elsevier, 539–574.
- Woolley M, Hamdan N and Kavazanjian E** (2021) The durability of EICP crusts subjected to ultraviolet (UV) radiation. Proceedings of the 20th International Conference on Soil Mechanics and Geotechnical Engineering.
- Zucca C, Fleiner R, Bonaiuti E and Kang U** (2022) Land degradation drivers of anthropogenic sand and dust storms. *Catena* **219**. <https://doi.org/10.1016/j.catena.2022.106575>.